Analyst

Accepted Manuscript

This article can be cited before page numbers have been issued, to do this please use: A. Reiner, N. G. Ferrer, P. Venugopalan, R. C. Lai, S. Lim and J. Dostalek, *Analyst*, 2017, DOI: 10.1039/C7AN00469A.

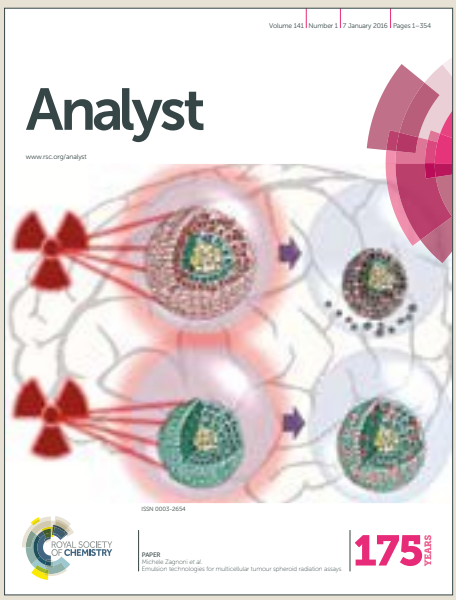

ROYAL SOCIETY OF CHEMISTRY

rsc.li/analyst

View Article Online
DOI: 10.1039/C7AN00469A

Magnetic nanoparticle-enhanced surface plasmon resonance biosensor for extracellular vesicle analysis

Agnes T. Reiner[a,b], Nicolas-Guillermo Ferrer-Sanchez[a], Priyamvada Venugopalan[a], Ruenn Chai Lai[b], Sai Kiang Lim[b], Jakub Dostálek[a]

[a] BioSensor Technologies, AIT-Austrian Institute of Technology GmbH, Muthgasse 11, 1190 Vienna, Austria

[b] Institute of Medical Biology, A*STAR, 8A Biomedical Grove, #06-06 Immunos, Singapore 138648

Corresponding Author:

Jakub Dostalek, PhD, E-mail: jakub.dostalek@ait.ac.at, Phone: +43 (0) 50550 4470, Fax: +43 (0) 50550 4450

Abstract

The sensitive analysis of small lipid extracellular vesicles (EVs) by using a grating-coupled surface plasmon resonance (GC-SPR) biosensor is reported. In order to enable the analysis of trace amounts of EVs present in complex liquid samples, the target analyte is pre-concentrated at the sensor surface by using magnetic nanoparticles and its affinity binding is probed by wavelength interrogation of SPR. The GC-SPR is demonstrated to allow for the implementation of efficient pulling of EVs to the sensor surface by using magnetic nanoparticles and an external magnetic field gradient applied through the sensor chip. This

View Article Online
DOI: 10.1039/C7AN00469A

approach overcomes slow diffusion-limited mass transfer and greatly enhances the measured sensor response. The specific detection of different EV populations secreted from mesenchymal stem cells is achieved with a SPR sensor chip modified with antibodies against the surface marker CD81 and magnetic nanoparticles binding the vesicles via annexin V and cholera toxin B chain.

Keywords: Surface plasmon resonance; diffraction grating; magnetic nanoparticles; biosensors; extracellular vesicles

1. Introduction

The analysis of extracellular vesicles (EVs) gains increasing interest in life sciences and medical research due to their multiple functions in cell communication in healthy but also in pathological state. EVs hold great potential in many clinical applications spanning from diagnostics and disease monitoring to the use for therapeutics and even as vaccines. However, this potential is hampered by the lack of specific, sensitive and reliable methods for their analysis. Currently used methods typically stem from those used in micro- or molecular biology for the analysis of cells. Hence, one of the biggest challenges for these methods is the small size of the lipid vesicles. For instance, a well-established method for cell analysis - flow cytometry - is only able to detect lipid vesicles bigger than ~ 200 nm which translates to the fact that the majority of EVs is actually not detected [1-3]. Another method employed for the analysis of small particles is nanoparticle tracking analysis (NTA). Similar to flow cytometry, NTA also relies on the light scattering properties of particles but allows for the detection of smaller particles because of the addition of a microscopy unit. However, due to the EVs' refractive index being very close to that of surrounding medium and their small size, they scatter light very weakly, which results in low signal-to-noise ratios. Nevertheless, it should

View Article Online
DOI: 10.1039/C7AN00469A

be noted that these methods are under constant development and dedicated flow cytometers with technical adjustments for EV analysis or the use of fluorescence detection have greatly improved their sensitivity for small EVs [3-6].

Complementary to flow cytometry and NTA that can analyze EVs in a solution, there are pursued optical biosensors for detection and observation of EVs that are captured at surfaces. Among these, surface plasmon resonance (SPR) based techniques are suitable for the optical probing of affinity binding of EVs by the tightly confined field of surface plasmons (SPs) travelling along metallic surfaces [7]. One of the first SPR biosensors employed a SPR imaging platform for parallelized detection of EVs on antibody microarrays [8]. Spots of antibodies specific for a selected set of proteins carried by EVs were used for screening of EV samples for potential cancer biomarkers. Another high throughput platform was presented by Im et al., who used a plasmonic chip with arrays of plasmonic nanoholes [9]. Antibodies specific for the tetraspanin protein CD63 [which can be found on EVs [10]] were used for sensitive detection of EVs and a limit of detection of 670 aM was reported for a sandwich assay amplified by metallic nanoparticles. By incorporation of several microfluidic channels, the sensor could be used to analyze multiple markers or samples in parallel. The plasmonic biosensor was demonstrated to offer superior sensitivity compared to regular heterogeneous assays based on enzyme-linked immunoassays (ELISA) and western blot.

Höök's group focused on quantitative direct measurements of EVs by a SPR biosensor [11]. The sensor surface was functionalized with an antibody against CD63 and the analysis of diffusion-limited binding kinetics enabled determining the concentration of EVs in a sample in the pM range. The performance of such a SPR biosensor was improved by probing the bound EVs by SPs resonantly excited at two different wavelengths [12]. With this platform it was possible to determine the EV concentration with a relative error of only 10 % compared to the earlier 50 %.

View Article Online
DOI: 10.1039/C7AN00469A

In general, all currently pursued EV SPR biosensors rely on diffusion-limited binding kinetics on the sensor surface. As EVs are objects with a size around 100 nm, their diffusion is slow and limits the yield in the collection of analyte on the sensor surface. Grating-coupled SPR with magnetic nanoparticle (MNP)-driven collection of protein analytes on the sensor surface was demonstrated to overcome such limitation for small protein molecules [13], and in particular for detection of large, slowly diffusing bacterial pathogens [14]. Both these works relied on the measurements of angular reflectivity spectra, which complicates the multiplexing of the assay and requires rotating of the sample. This paper presents a sensor that utilizes wavelength interrogation of SPR which provides the advantage of simpler operation. It is applied for the analysis of EVs exhibiting a diameter of about 100 nm with an enhanced sensor response by a combination of an increased mass transfer rate and amplified refractive index changes associated to analyte affinity binding. EVs are extracted and delivered to the sensor surface by their binding to MNPs via lipid-binding proteins, Annexin V (AV) and Cholera toxin B chain (CTB), and they are affinity captured by antibodies against CD81 at the SPR grating sensor surface.

2. Experimental

2.1 Materials

Polydimethylsiloxane elastomer (PDMS) Sylgard 184 was obtained from Dow Corning and the UV-curable polymer Amonil MMS 10 was from AMO GmbH. Dithiolalkanearomatic PEG3 with hydroxyl endgroup (SPT-0013) and the dithiolalkanearomatic PEG6 with carboxyl endgroup (SPT0014A6) were purchased from SensoPath Technologies. N-(3-Dimethylaminopropyl)-N'-ethylcarboddiimide hydrochloride (EDC), N-Hydroxysuccinimide (NHS), ethanolamine and ethylenglycol, as well as acetic acid and sodiumacetate for the

View Article Online
DOI: 10.1039/C7AN00469A

preparation of acetate buffer were bought from Sigma-Aldrich. The mouse monoclonal antibody against human CD81 (1.3.3.22) and the HRP-conjugated goat anti-mouse secondary antibody (sc-2031) were purchased from Santacruz Biotechnology. Phosphate buffered saline (PBS) at a pH of 7.4 from Merck was used for the functionalization. PBS with addition of 0.05% Tween 20 (Sigma-Aldrich) only (PBST) or with 0.05% Tween 20 and 0.1% bovine serum albumine (Life Technologies) (PBSTB) were used as running buffers for the MNP-enhanced SPR measurements. The ligands CTB (SBL Vaccin AB) and AV (Biovision) for pre-incubation with EVs were biotinylated with Sulfo-NHS Biotin (Thermo Fisher Schientific). MNPs with a diameter of 200 nm and coated with streptavidin (fluidMAG-Streptavidin) were purchased from Chemicell. Prior to the use, streptavidin coated MNPs were washed twice with PBSTB by applying a magnetic field for separation of the MNPs from the solution. For the CD81-ELISA Dynabeads M280 Streptavidin and Amplex Red Substrate were purchased from Thermo Fisher Scientific.

2.2 Biological samples and EV characterization

We used EVs derived from mesenchymal stem cells (MSCs) that have been studied already in great detail [15-17]. EVs were obtained from the conditioned medium of MSCs. The cell cultivation and EV isolation were pursued as described earlier [17]. In short, conditioned medium was harvested after 3 days of cell growth and concentrated 100x for EVs by tangential flow filtration. Sample aliquots were stored at -80 °C. The total protein concentration was assessed by Coomassie Plus (Bradford) Assay (Thermo Fisher Scientific) and used as a surrogate for EV concentration. In addition the particle number in the EV samples was measured by NTA using the ZetaView instrument (ParticleMetrix) according to manufacturer's instructions. In brief, the EVs were diluted to a concentration of 0.5 µg/ml with 0.22µm filtered PBS and analyzed. The instrument setting were as following: the sensitivity was set to 90, the shutter to 30, maximal size was set to 1000 and minimal size to

View Article Online
DOI: 10.1039/C7AN00469A

5, minimal brightness was set to 25, and measurement mode was size distribution at 1 cycle and 11 positions. After the measurement, the raw data was analyzed with the software ZetaView 8.03.08.

The EV samples were further characterized for their CD81 concentration in the CTB- and AV-binding subpopulation by an ELISA on MNPs, that was performed as described earlier [17]. Briefly 0.1 or 1 µg of MSC-derived EVs were incubated with 250 ng biotinylated CTB or AV, respectively. After 30 min incubation 30 µl of washed Dynabeads M280 Streptavidin were added and incubated for 30 min again. The MNPs with bound EVs were then washed twice and incubated with anti-CD81 antibodies, washed again and incubated with HRP-conjugated goat anti-mouse secondary antibodies. The HRP activity was determined using Amplex Red Substrate as per manufacturer's instructions. A biotinylated-CD81 peptide was used as standard. The concentration is given as ng of CD81 per µg total protein of the MSC-EV sample used for the EV coupling to the MNPs.

2.3 Preparation of GC-SPR sensor chips

A linear relief sinusoidal grating was prepared by UV laser interference lithography and their multiple copies were made by soft lithography as described before [18]. Briefly, a structure with a period of Λ=430 nm and modulation depth of d=60 nm was casted to PDMS, which was cured for 3 days at room temperature before it was used as a working stamp. Cleaned BK7 glass substrates were coated with the UV-curable polymer Amonil MMS 10 by spin-coating at 3000 rpm for 120 s. Then, the PDMS working stamp was placed on the top of the Amonil surface and irradiated by UV light (UV lamp Bio-Link 365, Vilber Lourmat). Finally, the PDMS stamp was detached from the cured Amonil MMS 10 leaving a copy of the master structure on the glass substrate. The copied gratings were subsequently coated with 4 nm of chromium and 100 nm of gold by vacuum thermal evaporation (HHV AUTO 306 from HHV LTD) in vacuum better than 10^{-6} mBar.

View Article Online
DOI: 10.1039/C7AN00469A

2.4 Optical system

A flow-cell was clamped against the grating sensor chip and it consisted of a polished glass substrate with drilled input and output ports and a thin PDMS gasket. The volume of the flow-cell was of about 10 μL and analyzed liquid samples were flowed through by using the peristaltic pump REGLO Digital MS-4/8 (ISMATEC). The sensing spot in the flow-cell was illuminated with a polychromatic beam with a diameter of about 5 mm. The beam was emitted from a halogen bulb light-source (LSH102 from LOT-Oriel) and coupled to a multimode optical fiber (M25L02 from Thorlabs). The beam at the fiber output was collimated by using a lens (f=30 mm from Melles Griot) and subsequently passed through a polarizer and a cube beam-splitter (CM1-BS013 from Thorlabs). Then, the beam was made normally incident at the gold grating surface through the flow-cell and the reflected beam was separated at the beam splitter, coupled to a multimode optical fiber (M26L02 from Thorlabs) by using a collimator (F810SMA-635 from Thorlabs), and delivered to a spectrometer (HR4000 from Ocean Optics). The wavelength spectrum of the reflected light was measured for transversally magnetic polarization (TM) and normalized with that acquired for transversally electric polarization (TE). The normalized reflectivity TM/TE spectra with a SPR dip located at a wavelength of about 640 nm were processed by a dedicated software developed in-house by using LabView (National Instruments). In order to track the SPR wavelength in time, the sequentially acquired spectra were fitted in a selected wavelength range with a polynomial function. The SPR wavelength λ_{SPR} was determined as the minimum of the fitted analytical function with a repetition time of about 5 sec. On the opposite side of the flow cell, a cylindrical permanent magnet (NdFeB with diameter of 10 mm and length of 35 mm from Neotexx) was approached to the grating sensor chip in order to attract MNPs at

View Article Online
DOI: 10.1039/C7AN00469A

its surface. The optical system and assay setup including sample pre-incubation and details on the sensor surface architecture for affinity binding of the analyte are illustrated in Figure 1.

(The preferred position for Fig.1)

2.5 Functionalization of GC-SPR sensor chips

The gold-coated sensor chips were immersed in ethanol with thiols dissolved at 1 mM concentration in order to form a self-assembled monolayer (SAM). The solution contained a mixture of dithiol-PEG6 with carboxyl end group for later surface functionalization and dithiol-PEG3 with hydroxyl end group for passivation. The molar ratio of carboxyl to hydroxyl-terminated thiols was 1:9. After the overnight incubation, the sensor chips were thoroughly rinsed with ethanol, dried immediately in a stream of air and stored under argon atmosphere. The functionalization with a specific antibody against CD81 was performed *in situ* by amine coupling according to standard protocols. All solutions were flowed over the sensor surface at a constant speed of 30 µl/min. As a first step PBS was rinsed through the flow cell to reach a stable baseline in the sensor response $\lambda_{SPR}(t)$. Then, PBS spiked with 2 % ethylenglycol was flowed through, producing a refractive index change of 2×10^{-3} refractive index units (2 mRIU) in order to calibrate the sensor. Afterwards, sodium acetate buffer with a pH-value of 5 was flowed and the carboxyl groups on the surface were subsequently activated by the incubation with EDC and NHS for 15 min at concentrations of 0.4 M and 0.2 M, respectively. Then, the surface was rinsed with sodium acetate buffer and the specific antibody against CD81, diluted in the same buffer at a concentration of 25 µg/ml, was flowed for 10 minutes. Finally, ethanolamine at 1 M and pH of 8.5 was used to inactivate all remaining carboxyl groups before the buffer was changed again to PBS.

View Article Online
DOI: 10.1039/C7AN00469A

2.6 Detection assay

EVs were diluted in a total of 100 µl PBS and each sample was spiked with 250 ng of biotinylated CTB or AV and incubated for 30 min at room temperature on a shaker. Calcium containing buffer was added to the incubation mix when incubated with AV at a final calcium concentration of 2 mM. Then, 10 µg of washed streptavidin coated MNPs, corresponding to a number of ~$2.2 \cdot 10^9$ MNPs, were added to the EV-ligand-mix and incubated for 30 min at the same conditions as before to let EVs attach to the MNPs via the biotinylated lipid-binding proteins. Afterwards, the MNPs with bound EVs were collected from the sample and washed twice with PBSTB in order to remove any unbound EVs and other molecules. Finally, the MNPs were resuspended in 1 ml of PBSTB, leading to a MNP concentration of 10 µg/ml or ~3.6 pM, and analyzed with the GC-SPR biosensor. The amount of EVs is further quantified as amount of total protein in starting material of EVs diluted in 1 ml after the isolation procedure (ranging from 0.76 to 3.0 µg/ml). A MNP diameter of about 200 nm was chosen as they are sufficiently large for the manipulation with the used permanent magnet. In addition such diameter is comparable to the penetration depth of the surface plasmon field that probes the sensor surface. The used MNP concentration was optimized in order to maximize the measureable SPR response due to the affinity binding of target EV analyte at the sensor surface. For MNP concentrations below 10 µg/ml, the SPR response was decreasing with the MNP concentration (1 µg/ml, data not shown). For higher MNP concentrations, the sensor surface was blocked with the collected MNPs which hindered the affinity binding of target EV analyte at the sensor surface (100 µg/ml, data not shown). In addition, aggregation can be observed due to the multivalency of the MNPs and multiple binding sites available on the target EV analyte. In general, the aggregation was intended to be avoided by using a higher amount of MNPs in relation to the EV concentration, due to the fact that large aggregates tend

View Article Online
DOI: 10.1039/C7AN00469A

to clog the microfluidic chamber and bind outside the evanescent field of surface plasmons that probe the sensor surface.

Each sample was flowed across the sensor surface for 10 min with the magnetic field gradient applied by placing the permanent magnet in a distance of 5 mm from the sensor surface. The sensor surface was probed by resonantly excited SPs before and during collecting the MNPs and the SPR wavelength λ_{SPR} was tracked in time. Then the magnetic field was switched off by removing the magnet and the sensor surface was rinsed with PBSTB until a stable baseline in $\lambda_{SPR}(t)$ was reached again. Since the flow-cell was oriented in a vertical direction and the flow of liquid samples was directed upwards, the flow-cell had to be flushed shortly with PBSTB at high speed to remove all unspecifically attached MNPs and their aggregates.

The SPR signal $\lambda_{SPR}(t)$ was processed in the software Origin Pro. First the initial baseline was set to zero and it was normalized to the SPR response to a bulk refractive index change due to the spiking of PBS with 2 % ethylenglycol. SPR wavelength variations were converted to the unit of mRIU. The response to the affinity binding of MNP-bound EVs was determined as the sensor response difference between the baseline before the injection of a sample and after washing of the sensor surface with the magnetic field gradient switched off.

2.7 Observation of sensor chips

Atomic force microscopy (AFM) and scanning electron microscopy (SEM) were used to examine the biosensor surface before and after binding of MNP-bound EVs. For this purpose the functionalized sensor surface was exposed to either MNPs incubated only with the lipid-binding ligand as control or with MNPs incubated with ligand and EVs of different concentration. The assay was performed as described above, but in the end the flow cell was

View Article Online
DOI: 10.1039/C7AN00469A

rinsed with water and the sensor surface was dried in a stream of air immediately after removal of the flow cell.

To get a detailed height information of the MNPs on the grating structure, the AFM system Molecular Imaging PicoPlus was employed, which is a multipurpose, high resolution scanning probe microscope and was operated in tapping mode [19]. The SEM SUPRA 40 microscope by Zeiss was employed to study the surface topography, which generates images of a sample by scanning it with a focused beam of electrons [20].

3. RESULTS AND DISCUSSION

The resonant coupling to SPs on the gold diffraction grating is manifested as a narrow dip in the measured wavelength reflectivity spectrum. As can be seen in Figure 2A, this dip is centered at a wavelength of λ_{SPR}~637 nm when PBS is flowed over the gold surface covered with a mixed thiol SAM. The excitation of SPs is due to the first order diffraction coupling by the normally incident beam, which occurs at a wavelength where the phase matching condition $\lambda_{SPR}=\Lambda \cdot N_{SP}$ is fulfilled. The N_{SP} stands for the effective refractive index of SPs travelling along the gold surface in contact with the aqueous sample. The resonant wavelength λ_{SPR} shifts to longer wavelengths when the refractive index on the gold sensor surface is increased, e.g. due to the binding of biomolecules or EVs. From the perturbation theory follows that such variations can be approximated by the following expression [21], which holds, if the thickness of the layer in which the biomolecules bind is much smaller than the wavelength λ_{SPR}:

$$\delta\lambda_{SPR} = S_b \frac{4\pi}{\lambda_{SPR}} \sqrt{N_{SP}^2 - n_b^2} \cdot \Gamma \frac{\partial n}{\partial c}, \quad (1)$$

View Article Online
DOI: 10.1039/C7AN00469A

where S_b is the signal sensitivity to variations of the bulk refractive index n_b, Γ is the surface mass density of bound biomolecules, and constant $\partial n/\partial c=0.2$ mm^3 mg^{-1} for the majority of organic polymers [22]. The PBS bulk refractive index of $n_b=1.34$ was determined from the measured reflectivity spectrum which shows a sharp feature at the critical wavelength $\lambda_c=578$ nm, see Figure 2A. This feature occurs at $\lambda_c=\Lambda \cdot n_b$ where the first diffraction order falls after the horizon. Similarly, the effective refractive index of SPs was determined as $N_{SP}=1.49$. The bulk refractive index sensitivity S_b was obtained from the time kinetics measurements presented in Figure 2B when the PBS spiked with 2% ethylenglycol was flown across the sensor surface. This composition induces a refractive index increase of $\delta n_b=2\cdot10^{-3}$ refractive index units (RIU). From the measured corresponding shift $\delta\lambda_{SPR}=0.85$ nm the sensitivity was obtained as $S_b=\delta\lambda_{SPR}/\delta n_b=425$ nm RIU^{-1}. This value is similar to other GC-SPR sensors operated at a similar wavelength [21]. It is worth of noting that the developed sensor system allowed measuring the SPR wavelength with the standard deviation of $\sigma(\delta\lambda)\sim9\cdot10^{-3}$ nm which corresponds to the resolution of $2\cdot10^{-5}$ RIU.

(The preferred position for Fig.2)

3.1 Modification of the sensor chip with ligands

The sensor surface was functionalized with antibodies specific to the transmembrane protein CD81, which is a known marker for EVs in general [10] and for the used MSC-derived EVs in particular [17]. The ligand density on the sensor surface was controlled by the amount of carboxyl end groups present in the thiol SAM. Based on earlier optimization studies [23, 24] we chose a ratio of 1:9 for carboxyl to hydroxyl terminated thiols to avoid steric hindrance in binding of the target analyte due to a too high ligand density. In order to quantify the amount

View Article Online
DOI: 10.1039/C7AN00469A

of antibody on the sensor surface, the immobilization was performed *in situ* and the attachment of molecules to the surface was monitored with GC-SPR. A typical sensorgram in Figure 2B shows a strong shift in $\delta\lambda_{SPR}$ after injecting EDC/NHS at time t=23 min due to the bulk refractive index change. After the rinsing with acetate buffer at t=38 min, the SPR wavelength λ_{SPR} decreases to the original value. Then, anti-CD81 was flowed over the surface with activated carboxyl groups between t=40 and 50 min. The covalent binding of the antibody leads to a gradual shift in λ_{SPR} due to the increased surface mass density Γ. After the rinsing and passivating of unreacted carboxyl groups with ethanolamine at t=60 min, the difference in the SPR wavelength of $\delta\lambda_{SPR}$=1.58 nm was measured. By using equation (1), this shift can be translated to the surface mass density of immobilized antibody of Γ~1.5 ng mm^{-2} which is lower than a full packed monolayer [25, 26], because a lower concentration of carboxyl terminated thiols were used in the thiol SAM. This value is in aggreement with the surface mass density of 1.4-1.5 ng mm^{-2}, which performed best in capturing the target analyte, when different immobilization techniques for surface functionalization with antibodies were compared [27].

3.2 GC-SPR readout of MNP-enhanced EV assay

The herein used EVs are produced and isolated continuously from conditioned cell culture medium by tangential flow filtration and tested for total protein concentration and CD81 content in EV subpopulations by Bradford assay and ELISA, respectively. Since all cells secrete many different kinds of vesicles summarized as EVs, also in the MSC-EV sample several different vesicle populations could be isolated based on their binding to proteins with specific affinity to different lipids [17]. These EV populations are characterized by their distinct lipid and protein profile, which was used to test and develop the here presented EV analysis method.

View Article Online
DOI: 10.1039/C7AN00469A

Firstly, direct GC-SPR detection of all MSC-derived EVs without the isolation of subpopulations and binding to MNPs was tested. Samples with PBST used as running buffer and MSC-EVs diluted 100-, 1,000-, and 10,000-fold (resulting in a total protein concentration of 15, 1.5, and 0.15 μg/ml) were subsequently flowed over the sensor surface with anti-CD81 antibody. As seen in the inset of Figure 3A, the SPR signal was monitored in time and did not show a measurable direct response to the EV binding.

In order to enhance the GC-SPR sensor reponse, MNPs were employed for the more efficient collection of specific EV subpopulations at the sensor surface and to increase the binding-induced surface mass density Γ. In a pre-incubation step EVs were bound to MNPs and consecutively flowed across the sensor surface, while a magnetic field gradient was applied (see Figure 1). Due to the magnetic force experienced by the MNPs the bound EVs were accumulated on top of the functionalized surface. Afterwards, the magnetic field gradient was switched off by removing of the permanet magnet. Then, running buffer was rinsed and only affinity captured MNPs stayed on the surface that were bound via the CD81 present on the EVs' surface. It is worth of noting that without applying the magnetic field no measureable response was observed when flowing MNPs with or without bound EVs across the sensor surface.

A typical SPR sensorgram for the MNP-enhanced EV assay is presented in Figure 3A. Each measurement cycle consisted of a 10 min incubation step of MNPs with application of a magnetic field, followed by 20 min rinsing with buffer after removal of the magnetic force, and flushing the flow cell with running buffer at maximum flow rate to remove all weakly bound particle aggregates. To ensure that the MNPs were not unspecifically binding to the antibodies or irreversibly sticking to the sensor surface, control MNPs, which were incubated only with the biotinylated lipid-binding ligands (b-ligand, i.e. CTB or AV) without EVs, were rinsed across the surface as the first measurement cycle in each experiment. Only if the SPR

View Article Online
DOI: 10.1039/C7AN00469A

signal after the rinsing was equal to the baseline before the MNP incubation, indicating complete removal of MNPs from the sensor surface, the measurement was proceeded by incubation with MNPs pre-exposed to ligands and EVs.

As seen in Figure 3, the attraction of MNPs not incubated with EVs at the sensor surface is manifested by a decrease of the λ_{SPR} between t1 and t2 when the magnetic field gradient was applied. Interestingly, after the magnetic field is switched off at t2 the λ_{SPR} rapidly increases and then gradually shifts to the original baseline. Since the MNPs consist of a magnetite core, they strongly absorb light [28]. The associated decrease in reflected light intensity is more pronounced at shorter wavelengths compared to longer ones and lead to a flatter, broader and tilted SPR dip in the reflectivity spectrum (compare reflectivity spectra at t1 and t2 in Figure 3B). Particularly the increasing absoprtion with decreasing wavelength can be ascribed to a decrease of the determined λ_{SPR}. After the magnetic field is switched off, the majority of accumulated MNPs is quickly expelled from the sensor chip which is accompanied by an increase in the overall reflectivity signal and λ_{SPR}. The afterwards gradual decrease of the λ_{SPR} can be ascribed to the slow release of unspecifically adsorbed MNPs from the surface. When the same detection cycle is performed for a sample where MNPs are incubated with EVs, the sensor response differs (see Figure 3A, time t3-t5). Firstly, a λ_{SPR} increase is observed for the phase when MNPs are accumulated at the surface with the magnetic field applied (t3-t4). After the release of the MNPs by switching off the magnetic field, a stronger increase in λ_{SPR} is measured and almost no desorption is apparent. The overall decrease in the intensity of the reflected beam after the incubation with MNP-bound EVs and rinsing with buffer (compare reflectivity spectra at t3 and t5 in Figure 3B) supports the finding that the SPR response change $\delta\lambda_{SPR}$ is caused by MNPs binding to the surface via the captured EVs rather than free vesicles or proteins. Only if the MNPs do not carry EVs, the intensity of the collected light

View Article Online
DOI: 10.1039/C7AN00469A

goes back to its original level after removal of the magnetic field and rinsing (compare reflectivity curves measured at t1 and t3 in Figure 3B).

(The preferred position for Fig.3)

The experiment presented in Figure 3 shows that the employment of the MNP-based collection of EVs on the GC-SPR sensor surface allows enhancing the sensor response and observing the affinity binding of EVs at concentrations for which the direct detection assay is not sufficiently sensitive. Furthermore, it has to be taken into consideration that the indicated concentration of MNP-bound EVs is the total protein amount, used as input for the pre-incubation, divided by the volume of buffer used for resuspension of the MNPs after EV isolation. Hence this is the maximum concentration of EVs or protein that could be present on the MNPs. The actual concentration is most likely lower than this, because only a subpopulation of EVs, that is specifically binding to the ligands, is bound to the MNPs. Consequently, the MNP-enhanced assay can detect EVs at even lower concentrations. In order to quantify the EV samples further, NTA was used and a particle count of 1.1-1.4·10^8 particles per µg of total protein in the EV sample was determined. From this the total protein concentration in the MNP-bound EV samples can be converted to molar concentrations. Using the MNP-enhanced GC-SPR assay CD81-carrying EVs were detectable down to a concentratin of 0.76 ng/ml or 130 fM. Again it has to be emphasised that this is the maximum possible concentration of EVs in the MNP-bound sample, hence the actual concentration that is detectable by these means is most likely lower. Other plasmonic biosensors for EV analysis shows detectable EV concentrations ranging from 670 aM to 2 pM with the similar SPR signal resolution in the µRIU range [8, 9, 11]. As the used materials and methods, including EV source, isolation and characterization, detection assay, and optical

View Article Online
DOI: 10.1039/C7AN00469A

setup and instruments, substantially differ, a direct comparison between these methods is rather complex task. In general, the combination of the earlier used methods with the herein presented MNP-capturing and collection of EVs by magnetic forces at the sensor surface could enhance the sensitivity of all of the different approaches.

In order to confirm that the SPR response change is related to the density of MNPs and captured EVs binding to the surface, we performed AFM and SEM of the sensor chips after the SPR assay. The high resolution AFM image of a sensor surface with captured MNPs clearly shows the accumulation of MNPs on top of the grating structure of the biosensor chip (see Figure 4A). As expected, the features bound to the surface exhibit a height of ~200 nm which agrees with the diameter of the used MNPs. Probably due to the partial aggregation of MNPs and EVs, actual counting of the particles and thus quantification of the density was not possible, but SEM images examining a wider area show clearly that many more particles are bound on the surface exposed to MNP-bound EVs (Figure 4B) compared to the surface exposed to control MNPs (Figure 4C). Additionally, this observation confirms the specificity of the functionalized surface to only bind EVs and not MNPs. On the one hand, the aggregation of the MNPs can be due to the binding of several MNPs to multiple binding sites on one molecule, e.g. multiple biotins on the lipid-binding ligands CTB and AV and multiple ligands on each EV. On the other hand, the MNP aggregation can also occur when very strong magnetic forces are applied to the MNPs resulting in irreversible aggregation [29].

(The preferred position for Fig.4)

View Article Online
DOI: 10.1039/C7AN00469A

3.3 Discrimination between AV- and CTB-binding EVs

To further examine the capabilities of this assay, the binding of different EV populations on the anti-CD81 functionalized sensor surface was investigated. For this purpose different amounts of MSC-derived EVs were incubated either with biotinylated AV or CTB, bound to MNPs, and consecutively analyzed with the MNP-enhanced SPR assay. As illustrated in Figure 5A the CTB-binding EVs were binding to the anti-CD81 antibodies on the sensor surface and the SPR response change increased in a concentration dependent manner (linear regression between 0.76 and 3.0 µg/ml EVs with Pearson R = 0.999). However for the AV-binding EVs no binding to the surface was observable even at higher concentrations, because they express CD81 only at a very low concentration compared to the CTB-binding EVs [17]. These results prove that the MNP-enhanced assay is capable of specifically detecting different EV populations based on their surface marker expression.

For further quantification and validation of these results, the CD81 concentration in CTB- and AV-binding EVs was determined by ELISA performed on MNPs. As displayed in Figure 5B the CTB-binding EVs carry ~8.0 ng of CD81 per µg of total protein of the EV sample used for the binding to the MNPs. The CD81 content of AV-binding EVs, in contrary, is barely detectable and lies at ~0.2 ng per µg total protein of EVs. Hence we were able to detect CD81-carrying EVs with the MNP-enhanced assay down to a concentration of 6 ng CD81/ml in the CTB-binding EVs.

(The preferred position for Fig.5)

View Article Online
DOI: 10.1039/C7AN00469A

4. CONCLUSIONS

A new plasmonic biosensor for the analysis of EVs based on GC-SPR with wavelength interrogation is presented. The sensor makes use of the highly efficient accumulation of EVs on the sensor surface by their coupling with MNPs and applying a magnetic field gradient. This approach was demonstrated to enhance the SPR sensor response by a combined effect of increased speed of binding kinetics and enhanced surface mass density. The analysis of EVs secreted by mesenchymal stem cells at concentrations down to 0.76 µg/ml or 130 fM (quantified as total protein concentration or by nanoparticle tracking analysis, respectively) was achieved, which was not possible for direct SPR detection format or the sandwich MNP assay without active magnetic pulling. Through functionalization of the sensor with antibodies specific for CD81, specific detection of EV subpopulations isolated with lipid-binding ligands CTB and AV with the MNP enhanced GC-SPR assay was achieved. We believe that this detection platform may provide attractive means for rapid highly parallelized screening of EV-based biomarkers by e.g. grating-coupled SPR imaging [30]. In addition, by the use of grating-coupled surface plasmon enhanced fluorescence [18], detection sensitivity can be further pushed forward and enable analysis of minute amounts of cancer-specific EVs in complex samples such as blood plasma.

Acknowledgment

ATR was supported by the Austrian Federal Ministry for Transport, Innovation and Technology (GZ BMVIT-612.166/0001-III/I1/2010) via the International Graduate School Bio-Nano-Tech [a joint Ph.D. program of the University of Natural Resources and Life Sciences Vienna (BOKU), the Austrian Institute of Technology (AIT), and the Nanyang Technological University (NTU)] and by the Institute of Medical Biology of the Agency for

View Article Online
DOI: 10.1039/C7AN00469A

Science, Technology and Research (A*STAR). PV acknowledges support from Austrian Science Fund (FWF) under the grant agreement I 2647. NGFS acquired support from Erasmus Plus.

Declaration of Interest

The authors declare no conflict of interest.

View Article Online
DOI: 10.1039/C7AN00469A

References

1. E. van der Pol, F. A. Coumans, A. E. Grootemaat, C. Gardiner, I. L. Sargent, P. Harrison, A. Sturk, T. G. van Leeuwen and R. Nieuwland, *Journal of thrombosis and haemostasis : JTH*, 2014, **12**, 1182-1192.

2. N. Arraud, C. Gounou, R. Linares and A. R. Brisson, *Journal of thrombosis and haemostasis : JTH*, 2015, **13**, 237-247.

3. N. Arraud, C. Gounou, D. Turpin and A. R. Brisson, *Cytom Part A*, 2016, **89A**, 184-195.

4. E. J. van der Vlist, E. N. Nolte-'t Hoen, W. Stoorvogel, G. J. Arkesteijn and M. H. Wauben, *Nature protocols*, 2012, **7**, 1311-1326.

5. V. Pospichalova, J. Svoboda, Z. Dave, A. Kotrbova, K. Kaiser, D. Klemova, L. Ilkovics, A. Hampl, I. Crha, E. Jandakova, L. Minar, V. Weinberger and V. Bryja, *Journal of extracellular vesicles*, 2015, **4**, 25530.

6. L. Pasalic, R. Williams, A. Siupa, H. Campbell, M. J. Henderson and V. M. Chen, *Nanomedicine : nanotechnology, biology, and medicine*, 2016, **12**, 977-986.

7. A. T. Reiner, K. Toma, A. R. Brisson, D. Pils, W. Knoll and J. Dostalek, in *Frontiers in Biophotonics for Translational Medicine, Progress in Optical Science and Photonics*, ed. D. U. S. Olivo M., Springer Science+Businesse Media Singapore, Singapore, 2016, pp. 249-272.

8. L. Zhu, K. Wang, J. Cui, H. Liu, X. Bu, H. Ma, W. Wang, H. Gong, C. Lausted, L. Hood, G. Yang and Z. Hu, *Anal Chem*, 2014, **86**, 8857-8864.

9. H. Im, H. Shao, Y. I. Park, V. M. Peterson, C. M. Castro, R. Weissleder and H. Lee, *Nat Biotechnol*, 2014, **32**, 490-495.

10. M. Colombo, G. Raposo and C. Thery, *Annual review of cell and developmental biology*, 2014, **30**, 255-289.

11. D. L. Rupert, C. Lasser, M. Eldh, S. Block, V. P. Zhdanov, J. O. Lotvall, M. Bally and F. Hook, *Anal Chem*, 2014, **86**, 5929-5936.

View Article Online
DOI: 10.1039/C7AN00469A

12. D. L. Rupert, G. V. Shelke, G. Emilsson, V. Claudio, S. Block, C. Lasser, A. Dahlin, J. O. Lotvall, M. Bally, V. P. Zhdanov and F. Hook, *Anal Chem*, 2016, DOI: 10.1021/acs.analchem.6b01860.

13. Y. Wang, J. Dostalek and W. Knoll, *Analytical Chemistry*, 2011, **87**, 6202–6207.

14. Y. Wang, W. Knoll and J. Dostalek, *Analytical Chemistry*, 2012, **84**, 8345-8350.

15. R. C. Lai, F. Arslan, M. M. Lee, N. S. Sze, A. Choo, T. S. Chen, M. Salto-Tellez, L. Timmers, C. N. Lee, R. M. El Oakley, G. Pasterkamp, D. P. de Kleijn and S. K. Lim, *Stem cell research*, 2010, **4**, 214-222.

16. S. S. Tan, Y. Yin, T. Lee, R. C. Lai, R. W. Yeo, B. Zhang, A. Choo and S. K. Lim, *Journal of extracellular vesicles*, 2013, **2**.

17. R. C. Lai, S. S. Tan, R. W. Yeo, A. B. Choo, A. T. Reiner, Y. Su, Y. Shen, Z. Fu, L. Alexander, S. K. Sze and S. K. Lim, *Journal of extracellular vesicles*, 2016, **5**, 29828.

18. M. Bauch, S. Hageneder and J. Dostalek, *Opt Express*, 2014, **22**, 32026-32038.

19. R. Hiesgen, Haiber, J., in *Encyclopedia of Electrochemical Power Sources*, ed. J. Garche, Elsevier, Amsterdam, 2009, pp. 696-717.

20. M. T. Postek, Howard, K.S., Johnson, A.H., McMichael, K.L., *Scanning Electron Microscopy a student's handbook*, 1980.

21. P. Adam, J. Dostalek and J. Homola, *Sensor Actuat B-Chem*, 2006, **113**, 774-781.

22. G. L. Perlmann, L., *J. Am. Chem. Soc.*, 1948, **70**, 2719-2724.

23. W. Knoll, M. Zizlsperger, T. Liebermann, S. Arnold, A. Badia, M. Liley, D. Piscevic, F. J. Schmitt and J. Spinke, *Colloid Surface A*, 2000, **161**, 115-137.

24. J. Lahiri, L. Isaacs, J. Tien and G. M. Whitesides, *Analytical Chemistry*, 1999, **71**, 777-790.

25. A. Kausaite-Minkstimiene, A. Ramanaviciene, J. Kirlyte and A. Ramanavicius, *Analytical Chemistry*, 2010, **82**, 6401-6408.

26. J. Voros, *Biophys J*, 2004, **87**, 553-561.

27. S. K. Vashist, C. K. Dixit, B. D. MacCraith and R. O'Kennedy, *Analyst*, 2011, **136**, 4431-4436.

View Article Online
DOI: 10.1039/C7AN00469A

28. M. R. Querry, *Optical Constants*, U. D. o. Defense, Defense Technical Information Center, 1985.

29. J. Faraudo, J. S. Andreu and J. Camacho, *Soft Matter*, 2013, **9**, 6654-6664.

30. J. Dostalek, J. Homola and M. Miler, *Sensor Actuat B-Chem*, 2005, **107**, 154-161.

View Article Online
DOI: 10.1039/C7AN00469A

Figure captions:

Fig. 1 Schematics of the GC-SPR sensor system and developed assay. (A) shows the pre-incubation of extracellular vesicles (EVs) with the biotinylated lipid-binding ligand (b-ligand) and streptavidin (SA) coated magnetic nanoparticles (MNPs). (B) illustrates the surface chemistry used at the gold chip sensor surface for affinity binding of the target analyte. C depicts the optical setup of the MNP-enhanced GC-SPR assay and the system that allows the pulling of the target analyte to the sensor surface. SAM = thiol self assembled monolayer, Au = gold, SP = surface plasmon, L = lens, POL = polarizer, BS = beam splitter, GC-SPR = grating coupled surface plasmon resonance.

Fig. 2 Wavelength reflectivity spectra (A) and SPR sensorgram (B) for a representative example of immobilizing antibodies against CD81 onto the grating-coupled SPR sensor chip. The black spectrum in (A) is taken at the PBS baseline at the beginning of the measurement and the red spectrum is acquired at the end of the measurement after the binding of the anti-CD81. $\delta\lambda_{SPR}$ refers to the SPR response change caused by antibody binding to the surface. mRIU = milli refractive index unit, PBS = phosphate buffered saline, EG = ethylenglycol.

Fig. 3 Magnetic nanoparticle (MNP)-enhanced assay measurement. (A) Representative example of a SPR sensorgram for negative control MNPs without extracellular vesicles (EVs) and affinity binding of MNP-captured EVs at the sensor surface functionalized with anti-CD81 antibodies. MNPs were collected on the sensor surface by a magnetic field gradient (indicated as "+B"), after incubation of 10 min the magnetic field was removed ("-B") and unbound MNPs were washed away. $\delta\lambda_{SPR}$ refers to the SPR response change caused by MNP-bound EVs binding to the surface. The inset shows the SPR sensorgram for direct EV detection without MNP enhancement, when EVs were diluted to comparable concentrations and exposed to the same surface as in the MNP-enhanced assay. (B) Wavelength reflectivity

View Article Online
DOI: 10.1039/C7AN00469A

spectra from different time-points during the MNP-enhanced assay (indicated as t1 to t5 in A). mRIU = milli refractive index units, PBST or PBSTB = phosphate buffered saline with Tween 20 or Tween 20 and bovine serum albumin.

Fig. 4 AFM and SEM observation of sensor chips after the magnetic nanoparticle (MNP)-enhanced assay. An AFM image of GC-SPR sensor chip incubated with MNP-bound EVs (EV concentration 3 µg/ml) is shown in A. The grating structure of the surface with a modulation depth of about 60 nm and the bound MNPs with an approximate height of 200 nm can be seen. SEM images of the same chip as in A and of a sensor chip incubated with MNPs exposed to the lipid-binding ligand only are shown in B and C, respectively.

Fig. 5 CD81 detection in CTB- and AV-binding EVs. A SPR response change for different concentrations of CTB-binding EVs and AV-binding EVs captured by anti-CD81 antibodies on the sensor surface of the magnetic nanoparticle (MNP)-enhanced GC-SPR assay. B CD81 concentration of CTB- and AV-binding EVs measured by MNP-coupled CD81-ELISA, concentration is given as ng CD81 per µg total protein of EVs used for binding to the MNPs. mRIU = milli refractive index units, EVs = extracellular vesicles, CTB-EVs = cholera toxin b chain-binding EVs, AV-EVs = annexin V-binding EVs.

View Article Online
DOI: 10.1039/C7AN00469A

Fig.1

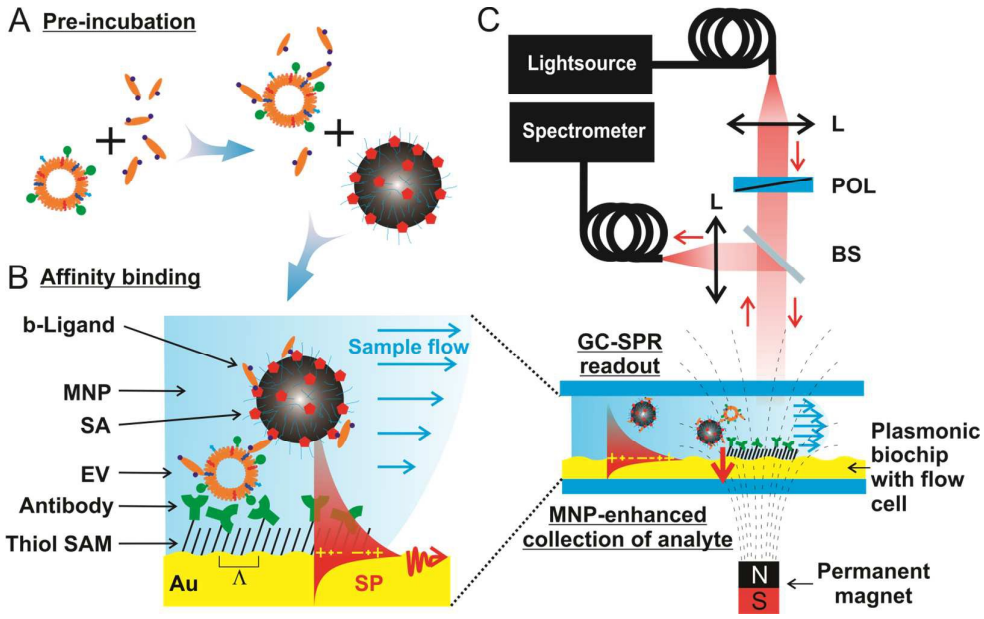

View Article Online
DOI: 10.1039/C7AN00469A

Fig.2

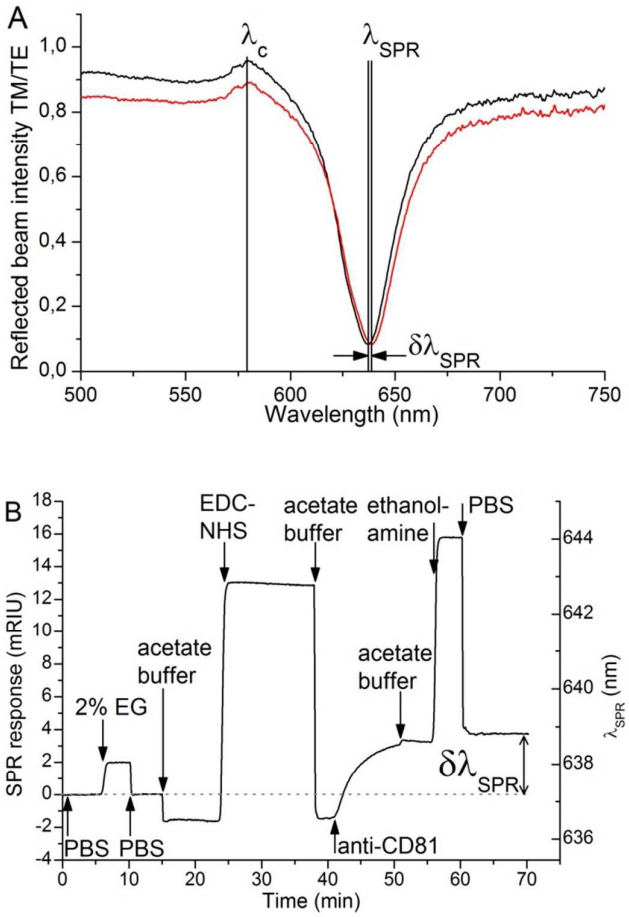

View Article Online
DOI: 10.1039/C7AN00469A

Fig.3

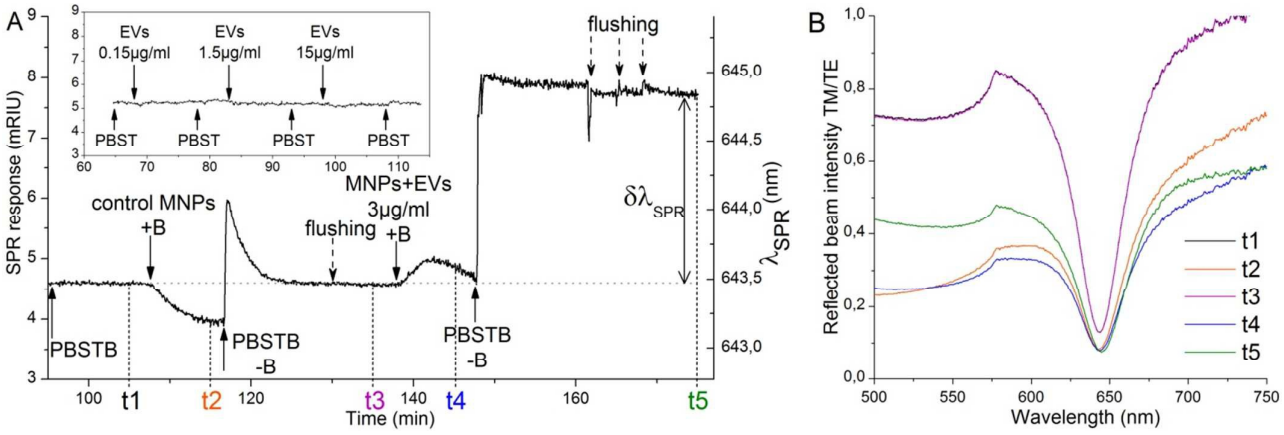

View Article Online
DOI: 10.1039/C7AN00469A

Fig.4

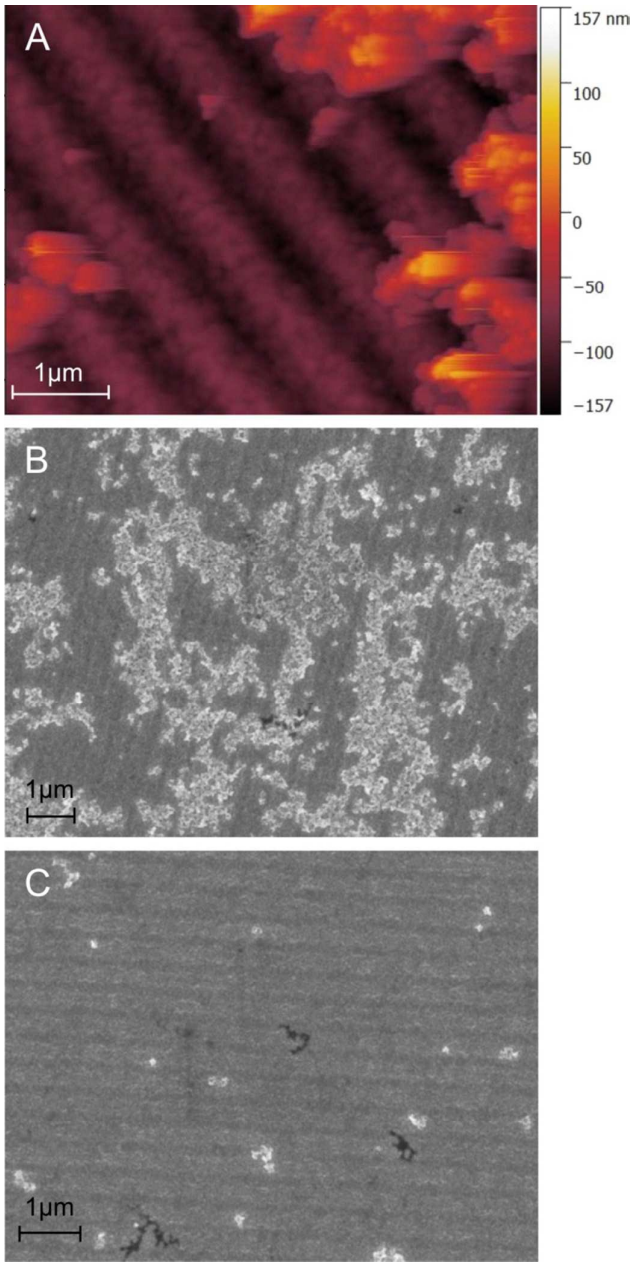

View Article Online
DOI: 10.1039/C7AN00469A

Fig.5